frontiers | Frontiers in Marine Science

TYPE Original Research
PUBLISHED 29 August 2025
DOI 10.3389/fmars.2025.1645286

OPEN ACCESS

EDITED BY
Eric Chassignet,
Florida State University, United States

REVIEWED BY
Tien Anh Tran,
Seoul National University, Republic of Korea
Donglai Gong,
College of William & Mary, United States

*CORRESPONDENCE
Tal Ezer
tezer@odu.edu

RECEIVED 11 June 2025
ACCEPTED 08 August 2025
PUBLISHED 29 August 2025

CITATION
Ezer T (2025) Surface currents in the Mid-Atlantic Bight: the role of the Gulf Stream versus wind.
Front. Mar. Sci. 12:1645286.
doi: 10.3389/fmars.2025.1645286

Surface currents in the Mid-Atlantic Bight: the role of the Gulf Stream versus wind

Tal Ezer*

Center for Coastal Physical Oceanography, Old Dominion University, Norfolk, VA, United States

Surface currents of the Mid-Atlantic Bight (MAB) were studied using high-frequency radar (HFR) observations at 6 km resolution during a 5-year period (2020–2024). The study's focus on the role of the Gulf Stream (GS) contrasts with most past studies that focused on the seasonal wind-driven currents. Empirical orthogonal function (EOF) analyses of the daily HFR currents were conducted with and without the GS, revealing modes of current variability linked to the seasonal wind pattern and storms versus modes linked to GS variability. The remote impact of the GS on coastal currents is complex, with different impacts seen on different parts of the MAB. For example, unusual GS meanders that move close to the coast impact flow variability near the shelf-break front, while other locations may be influenced by the strength of the GS and shift in the mean position of the GS. In general, it was found that monthly wind may be responsible for approximately 50%–80% of the surface current variability over the entire MAB, while the GS position and speed are correlated with the offshore component of the coastal currents and linked to approximately 10%–30% of the current variability. There are also large interannual variations, so that during some years, the GS impact on the coast is larger than during other years. Comparison between geostrophic velocity derived from altimeter data and the HFR surface currents shows the influence of the GS path on the offshore currents; however, close to the coast, the currents are wind- and river-driven, so that geostrophic currents obtained from altimeter data are not reliable. Therefore, combining altimeter and HFR data will provide a better current field than each data set alone. The study demonstrates the usefulness of the HFR data to study coastal dynamics and links between the coast and open ocean variability.

KEYWORDS

Mid-Atlantic Bight, Gulf Stream, high-frequency radar, surface currents, coastal dynamics

1 Introduction

The circulation and dynamics of the Mid-Atlantic Bight (MAB) between Cape Hatteras and Cape Cod have been studied for a long time using hydrographic observations, satellite data, and models (e.g., Beardsley et al., 1976; Beardsley and Winant, 1979; Beardsley and Haidvogel, 1981). The studies showed that the currents in the MAB are mostly driven by the wind, with strong winter winds from the northwest and weaker summer winds from the

southwest. The cold slope current from the north can also influence the circulation in the MAB and is part of the slope sea gyre (Figure 1a). Seasonal freshwater discharges from rivers affect the currents near the mouth of three main bays (Chesapeake Bay, Delaware Bay, and New York Bay; see Ezer and Updyke, 2025). For a more detailed review of the various past observations and the main dynamic features of the MAB, see Roarty et al. (2020).

High-frequency radars (HFRs) that can map surface currents within ~250 km from the coast have been used since the late 1990s. In the early to mid-2000s, a handful of radar stations were established in the MAB. Several stations have been added over the years, and at present, 36 stations are operated by the Mid-Atlantic Regional Association Coastal Ocean Observing System (MARACOOS) with an additional 4 along the Outer Banks of North Carolina operated by the Southeast Coastal Ocean Observing Regional Association (SECOORA; see Roarty et al., 2020). These stations provide surface current measurements at high temporal (hourly) and spatial (typically 1–6 km) range resolutions. Other gridded products, such as daily or monthly data, are also available. In the past, HFR observations were mostly used locally, for example, to study water exchange near a particular shelf and the impact of storms or to validate models (Kohut et al., 2006; Atkinson et al., 2009; Muscarella et al., 2011; Gopalakrishnan and Blumberg, 2012; Ezer et al., 2022; Han et al., 2022; Seim et al., 2022; Ezer and Updyke, 2024, 2025). Studies of surface currents using HFR were focused, for example, on the New Jersey shelf area (Gong et al.,

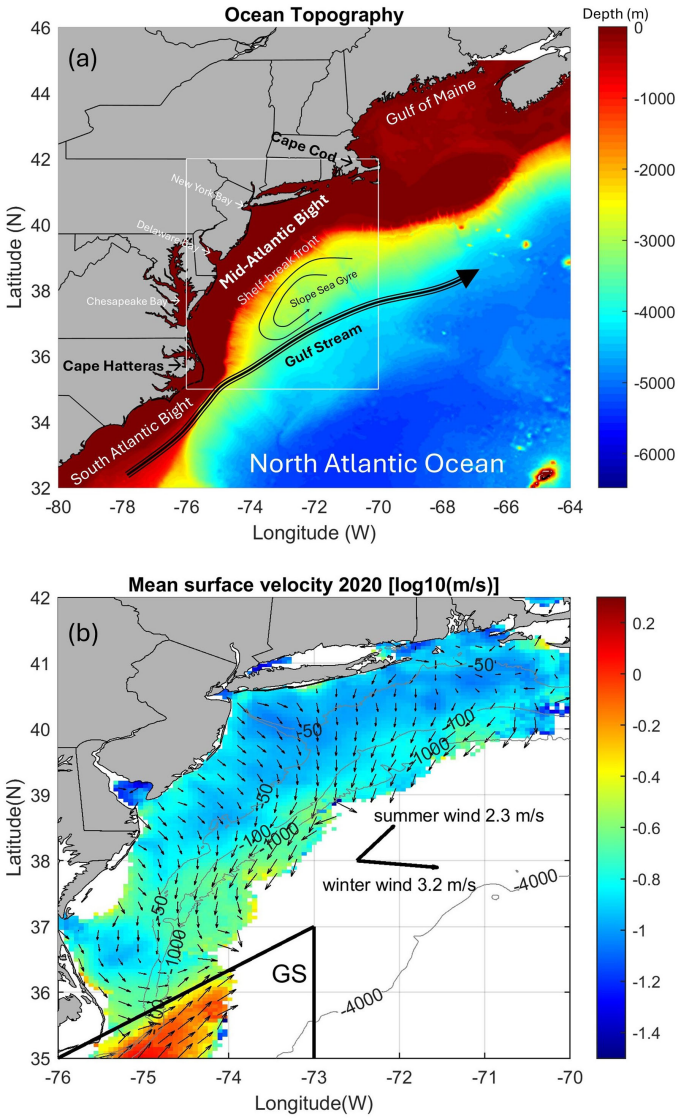

FIGURE 1
(a) A topographic and bathymetry map (ocean depth in m). The white box is the study area of the Mid-Atlantic Bight (MAB). Major topographic and oceanic features, as well as bays, are indicated. **(b)** An example of HFR currents showing the mean surface velocity speed (in color) and direction (vectors) during 2020. The current speed is in a log10 scale to show more details, and the vectors are shown every fourth point (about 24 km apart) for clarity. The heavy arrows in the center represent the mean winter wind (December–February, 2020) and mean summer wind (June–August, 2020) from the NOAA/NCEP monthly reanalysis. The triangle at the bottom-left is the area used to represent the Gulf Stream (GS) when separating the GS analysis from the "coastal region" (the rest). A few ocean depth contours (in m) are also shown.

2010; Dzwonkowski et al., 2009), looking at the seasonal wind-driven variations, spatial variations, and offshore transports. However, studies of the HFR currents over the entire MAB are rare—a recent example is the study of Roarty et al. (2020), which used hourly 6-km resolution HFR data over 2007–2016. Our study used similar data as Roarty et al., but for a more recent period (2020–2024) and with additional focus on the impact of the Gulf Stream (GS) relative to the better-known wind-driven forcing. Some studies used HFR data to study the GS position and variability and the connection between the GS and nearby currents (Haines et al., 2017; Muglia et al., 2022), but they focused only on the region near Cape Hatteras and did not try to link the GS to the entire MAB as done here. HFR data can also be used to correct along-track altimeter data near the coast (Roesler et al., 2013). However, the gridded 25-km resolution altimeter data that were used here to obtain the GS current and position are expected to be even less accurate than along-track data, especially near the coast. Some comparison between the HFR data and the altimeter data will show that combining the two data sets (HFR and altimeter) can be a good way to improve the dynamics that each data set alone can provide; this concept was demonstrated, for example, by Caballero et al. (2020).

The U.S. East Coast, with its large coastal population, is under threat of climate change and, especially, acceleration in flooding due to coastal sea-level rise (Ezer and Atkinson, 2014, 2017; Sweet and Park, 2014; Domingues et al., 2018; Ezer, 2022; Park et al., 2024). Therefore, numerous studies focused on links between coastal sea level and remote forcing such as the North Atlantic Oscillations (NAO; Hurrell, 1995), the Atlantic Meridional Overturning Circulation (AMOC, Smeed et al., 2014; Moat et al., 2023), and variations in the Gulf Stream (Ezer and Corlett, 2012; Ezer et al., 2013). Different mechanisms have been suggested to link open ocean variations in the Atlantic Ocean with coastal dynamics, such as Rossby waves, heat fluxes, and tropical storm interactions with ocean dynamics (Goddard et al., 2015; Little et al., 2019; Piecuch et al., 2019; Volkov et al., 2019, 2023; Dangendorf et al., 2021, 2023; Park et al., 2022, 2024). The motivation for this study comes from the fact that, unlike the numerous studies of remotely driven sea level (see above), not much is known about the potential impacts of open ocean dynamics on coastal currents, which have long been assumed to be mostly locally driven by winds and river flow. Recent studies of HFR surface currents near the mouth of Chesapeake Bay (Ezer, 2023a; Ezer and Updyke, 2024) as well as near the Delaware Bay and the New York Bay (Ezer and Updyke, 2025) suggest potential impacts from the NAO, AMOC, and GS. For example, variations in the GS may impact the outflow/inflow at the mouth of Chesapeake Bay, and NAO can affect decadal wind patterns and changes in precipitation that cause variations in river discharges (Rice et al., 2017). For more information, see also a recent review that summarized results from numerous studies of the GS over many years; some of these studies point to different processes that can link variations in the GS with coastal dynamics along the U.S. East Coast (Ezer, 2025). This study aims to extend the previous local studies of HFR surface currents near the mouth of bays into a study of the entire MAB to study potential mechanisms that link variations in the GS with coastal surface currents. Roarty et al. (2020), who used similar data (but for earlier years), mentioned the potential influence of the GS on surface currents, but with no specific analysis related to the GS. Therefore, more in-depth calculations, such as empirical orthogonal function (EOF) analysis, were conducted here to address the role of the GS in spatial and temporal patterns of surface currents. Gawarkiewicz et al. (2012) found that when a large GS meander moves closer to the shelf, it can result in unusual currents and extreme warming that influence marine life, but it is not clear if this is a one-time rare event or an oscillation pattern. The following analysis was able to partially address this issue as well as other patterns associated with wind and GS variations that affect the coastal currents.

The study is organized as follows. First, the data sources and analysis methods are described in Section 2, and then the results are presented in Section 3, focusing on wind and Gulf Stream impacts. Finally, the summary and conclusions are provided in Section 4.

2 Data sources and analysis methods

Hourly surface currents over the MAB at 6-km resolution for 2020–2024 were obtained from HFRs (https://hfrnet-tds.ucsd.edu/thredds/catalog.html). The data represent the flow of approximately the upper 2.5 m of the water column (though it is referred here and elsewhere as the "surface currents"). The raw data from multiple radars were combined to one gridded data set, and a 25-h running average filter was applied to the hourly archived data to remove daily wind and tide variability. Because of the spatial and temporal averaging and the fact that multiple overlapping radars were used, gaps in the data were very minimal and did not affect most of the results. From the hourly data, daily averages were obtained from 1 January 2020 to 31 December 2024. The HFR data used here for the entire MAB had the same resolution and area as the data used in Roarty et al. (2020), who described earlier data until 2016. Higher resolution (2-km) HFR data were used in recent studies, but only for limited regions near the mouths of bays (Ezer and Updyke, 2024, 2025); limited area HFR data were also used in other studies (Atkinson et al., 2009; Dzwonkowski et al., 2009; Gong et al., 2010; Muscarella et al., 2011; Gopalakrishnan and Blumberg, 2012; Ezer et al., 2022). The focus here on the entire MAB, using multiple HFRs along the coast, provides the capability to link the coastal currents with the GS.

To look at the seasonal and interannual wind-driven currents over the entire MAB, low-resolution (2.5° × 2.5°) monthly wind data of the area of interest (70–75°W, 35–42°N) were obtained from the NOAA/NCEP reanalysis (https://psl.noaa.gov/thredds/catalog/Datasets/catalog.html). Monthly mean geostrophic velocity data from satellite altimeters at 0.25° × 0.25° resolution were obtained from AVISO (https://www.aviso.altimetry.fr). Those products were processed by SSALTO/DUACS (Le Traon et al., 2003) and distributed with support from the Centre National d'études Spatiales (CNES). Geostrophic velocities for 2020–2022 were used, since the same analysis was done during these years (some analysis methods and formats of data were changed by AVISO in later years).

Sea surface temperature (SST) images from NOAA OISST V2.1 were obtained from https://climatereanalyzer.org/.

EOF analysis was used to analyze spatiotemporal variability in the surface current speed. A MATLAB code based on early atmospheric and climate data analysis (Bretherton et al., 1992) was used. Oceanographic applications of EOF include, for example, studies in the Gulf of Mexico (Oey et al., 2004). The analysis separated the current speed data $V(x,y,t)$ into spatial patterns ($EOFs$) and principal components (PCs) that show the time evolution of the amplitude of each EOF mode,

$$V(x,y,t) = \sum_{i=1}^{n} PC_i(t) \cdot EOF_i(x,y) \quad (1)$$

The analysis (Equation 1) also calculated the percentage of the total variability that is represented by each n mode. The spatial EOF pattern may suggest how different parts of the study area vary, and the time evolution may suggest variations in forcing, so the EOF analysis was compared with other data, such as wind, altimeter, and SST data. Correlations were calculated, for example, between the time evolution of the EOF and the time series of the mean GS current. Since the currents near the GS are much stronger than the currents near the coast, they dominate the mean current over the entire study area. Therefore, two separate EOF analyses were conducted: one for the entire region and one for the coastal region without the GS (see Figure 1b).

3 Results

3.1 Surface currents driven by the seasonal wind and storms

Figure 1b is an example of the typical annual mean flow (in this case, 2020), which is like the pattern previously described by Roarty et al. (2020) for an earlier period before 2017. The southeastward currents near the coast are driven by the outflow from three bays (Chesapeake Bay, Delaware Bay, and New York Bay; Figure 1a) and local wind (Muscarella et al., 2011; Roarty et al., 2020; Ezer and Updyke, 2024, 2025). Farther offshore, near the shelf-break front, the currents turn toward the southwest. A dominant feature is the northeastward flowing GS, with currents 5–10 times stronger than the coastal currents [see Haines et al. (2017) and Muglia et al. (2022) for details of the HFR observations of the GS near Cape Hatteras]. The mean surface current direction is generally to the right of the wind direction, as expected from the Ekman theory in the Northern Hemisphere (Ezer, 2023b). Roarty et al. (2020) used winds from NOAA stations near the observed currents, showing dominant southeastward winds that are stronger during the winter. The mean wind in 2020, shown in Figure 1b, is quite typical with strong winter winds toward the southeast and weaker summer winds toward the northeast. When the winds turn northeastward against the currents, the flow slows down, as shown by Roarty et al. (2020).

A Hovmöller diagram, i.e., mean currents as a function of longitude and time (Figure 2), shows the dominant role that the GS plays in the western part of the domain. However, the observations off Cape Hatteras captured changing portions of the GS, and in some years (approximately 2021–2022), the GS is barely visible in the HFR data. Also, during some periods, there are more intense currents over the entire region; these short-term events are related to storms, as discussed later. Because of the averaging process and the fact that multiple radars are used, gaps in the data are relatively small (mostly at the western and eastern edges of the domain), so they did not affect the results in a significant way.

When averaging the currents over the GS region and over the coastal region (see Figure 1b), it is difficult to find a significant

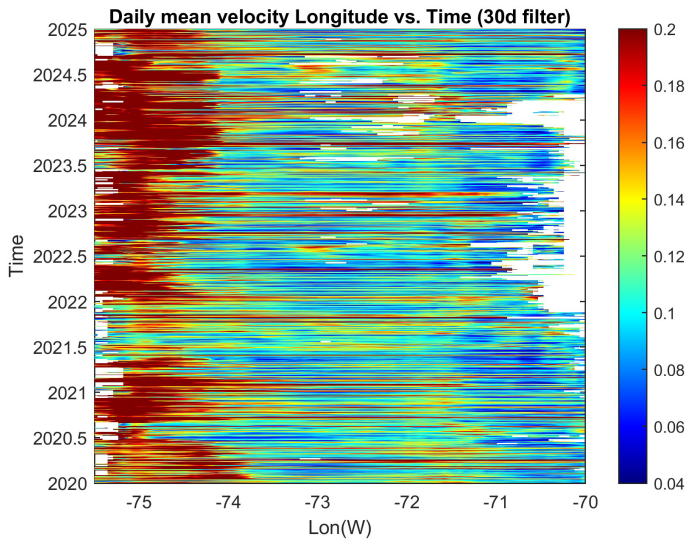

FIGURE 2
Hovmöller diagram of mean current velocity speed (in m/s) as a function of longitude and time obtained from north–south averaging all available data for each longitude. The red color west of ~74°W represents the high speed of the Gulf Stream. Time filter with a 30-day window was applied to remove some noise.

correlation because of the large random variations in the part of the GS captured by the HFR observations and missing data in 2021–2022 (Figure 3a). The mean coastal current, on the other hand, shows the expected seasonal cycle (red line in Figure 3b) with stronger currents during the winter when wind is stronger (Roarty et al., 2020). Daily peaks (green line in Figure 3b) are indications of storms passing the region (four significant storms are marked by A–D). An example of the impact of a storm (remnants of Hurricane Ian in early October 2022; D in Figure 3b) is shown in Figure 4. During the passage of the storm, the currents of the entire region turned toward the southwest before turning southeastward when approaching Cape Hatteras. The maximum surface velocity reached almost 1 m/s at the center of the MAB on October 3. After the storm passed, by October 8, the currents weakened, and close to the coast, they returned to their typical southeastward direction. In comparison, a past study of the HFR currents off the New Jersey coast during Tropical Storm Floyd in 1999 shows currents of up to ~0.40 m/s, but with significant impact from the large freshwater flux of this storm (Kohut et al., 2006).

Monthly wind speed over the region (Figure 5) shows a biannual pattern with the largest peak in the winter. This seasonal wind pattern drives the seasonal current pattern seen in Figure 3b. There are also significant interannual variations, with the strongest wind in 2021 and the weakest in 2020. The seasonal and interannual

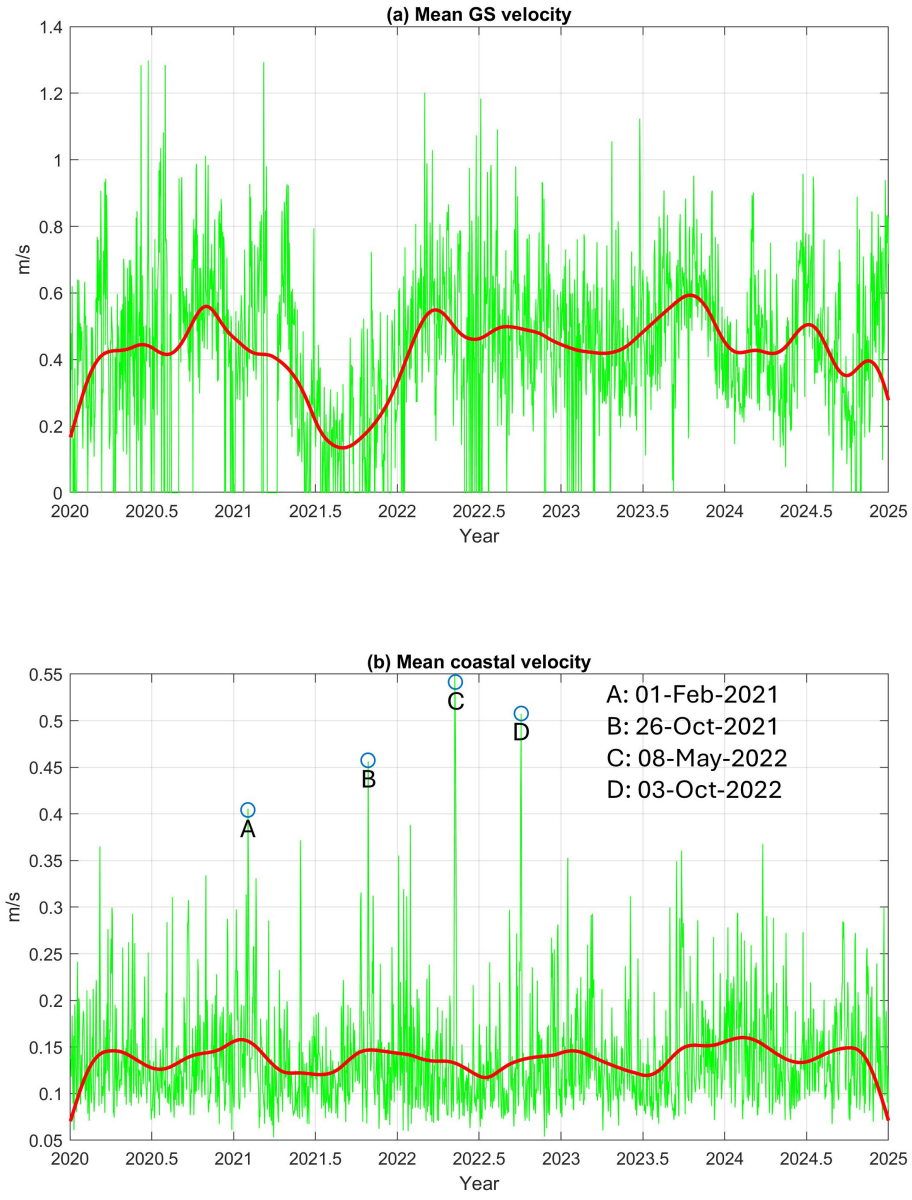

FIGURE 3
Mean surface current velocity calculated over **(a)** the Gulf Stream area (shown in Figure 1) and **(b)** the coastal area (excluding the GS). Green lines are daily values, and heavy red lines are after applying a 180-day filter. Extreme velocity peaks in **(b)** coincide with storms passing over the northeastern U.S.: A, the Groundhog Day Nor'easter; B, tropical storm Wanda and the "Bomb Cyclone"; C, extreme wind event that caused some tornados; and D, a cold front and remnants of Hurricane Ian.

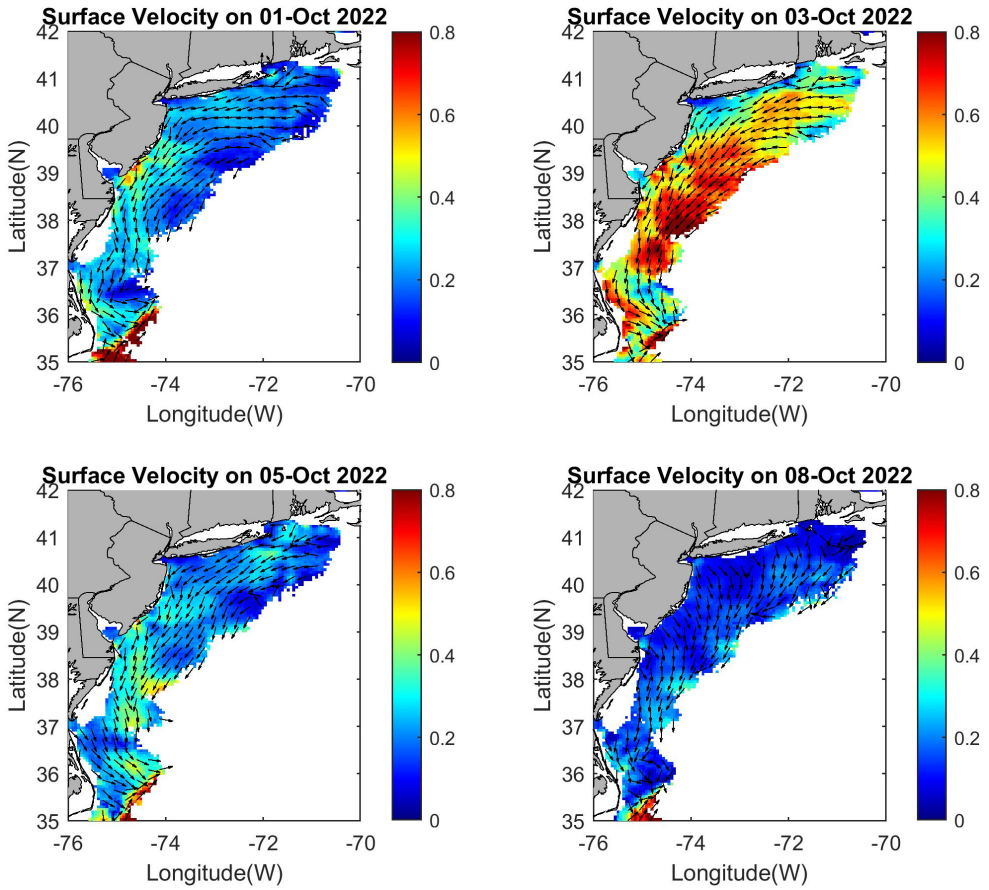

FIGURE 4
Examples of surface velocity (in m/s) during a storm—the remnants of Hurricane Ian in early October 2022 (see peak velocity D in Figure 3b). The current speed is shown in color and the current direction in vectors (every fourth grid point). Arrows are not proportional to speed for a clearer view of the areas with a weak velocity.

variations of the coastal currents (Figure 6; excluding the GS) and wind (Figure 7) are divided into a roughly offshore component (positive toward the southeast) and an alongshore component (positive toward the southwest). The mean coastal currents are fluctuating between southwestward and southeastward directions (left panels of Figure 6), with stronger offshore currents in the winter and fall and the strongest alongshore current in September–October; the latter may relate to tropical storms and hurricanes, as seen in Figure 4. There are also significant interannual variations in both the currents and the wind. For example, in 2021, the strongest offshore winter wind resulted in the strongest alongshore winter currents. In July 2022, an unusually strong northeastward wind (negative alongshore) reversed the alongshore current. These wind-driven coastal current variations are not unexpected and generally agree with past observations. The influence of seasonal and interannual variations in outflow from bays was also described before, showing that the impact is limited to the nearshore area (Roarty et al., 2020; Ezer and Updyke, 2025). While the influence of wind and river discharge on coastal currents was well described in past studies, studying the influence of the Atlantic Ocean and the GS on the coastal currents is more difficult and less understood. Therefore, a more complex analysis using EOF and additional satellite data was used in the next section to link the coastal currents with the GS.

3.2 EOF analysis of surface currents and links with Gulf Stream variability

EOF analysis of the 5-year daily data was first applied to the current speed of the entire region (coast and GS), and the first three modes are shown in Figure 8. These modes, which combined represent approximately 50% of the total variability, show a spatial pattern indicating variability where most of the area oscillates together (little variations within the coastal area), though the GS shows somewhat a larger response. The first two modes include seasonal variations and storms. For example, the large peaks in the time evolution of EOF Mode-2 (middle-right panel of Figure 8) correspond to the storms indicated in Figure 3b, and as shown in Figure 4, when a storm passed across the region, alongshore currents of the entire region increased. Moreover, the spatial pattern of EOF Mode-2 (middle-left panel of Figure 8) resembles the pattern of the storm's impact, with maximum currents at the center of the MAB (upper-right panel of Figure 4).

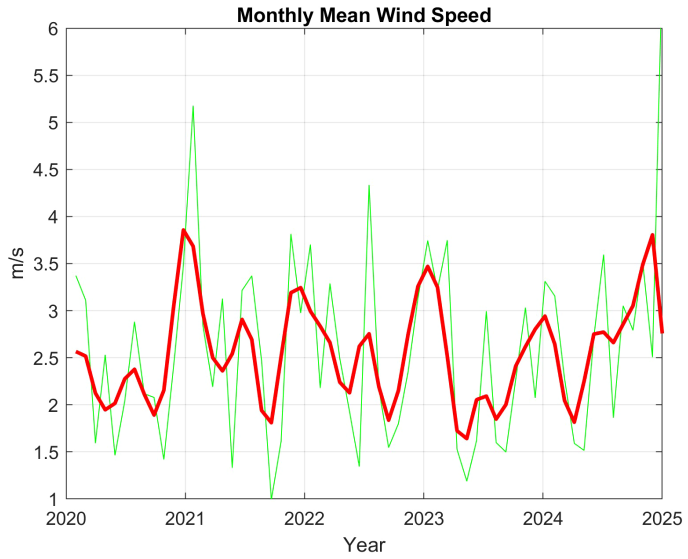

FIGURE 5
Monthly mean wind speed over the study area (green line) obtained from the NOAA/NCEP reanalysis, and the data after applying a 180-day filter (red line).

In EOF Mode-3 (bottom panel of Figure 8), the GS is in opposite phase to the rest of the MAB. Moreover, the time evolution shows almost no variability in mid-2021, when there were gaps in the GS data (Figures 2, 3a), thus suggesting that this mode represents GS-driven variability.

EOF Mode-4 to Mode-6, which combined represent approximately 10% of the total variability, indicate variability associated with the GS, so Figure 9 zooms in on the area near Cape Hatteras. The pattern of EOF Mode-4 and Mode-5 indicates variations in the position and strength across the GS, and Mode-6 may indicate variations along the GS. For example, the apparent weakening or reduced data of the GS approximately 2021 is also shown in the time evolution of Mode-6. As mentioned before, the HFR captured only a small part of the GS, so additional data will be assessed for the GS later.

The GS current is much stronger than the coastal currents (Figures 1b, 3) and, thus, overshadows the variability of the entire region. Therefore, a second EOF calculation is conducted using only the coastal currents without the GS area (excluding the triangle region in Figure 1b). The spatial pattern of the first 4 EOF modes, which combined are responsible for ~53% of the total coastal variability, is shown in Figure 10. Table 1 shows information on all the first 10 EOF modes; also shown in the table are the correlations between the time evolution of the EOF amplitudes and the time series of the mean velocity over the GS (Figure 3a) and over the coast (Figure 3b). Only Mode-1, representing 37% of the total variability, is highly correlated (R = 0.94) with the mean velocity over the entire coast, while almost all the other modes show a higher correlation of the EOF modes with the GS variability than with the coastal variability. Note that the EOF analysis in Figure 10 excludes the GS region, so that this correlation represents the remote influence of the GS on the coast. The impact of the GS seems complex as it spreads over several modes, each contributing only a small portion of the total variability and possibly affecting different subregions of the MAB. Summing up all the GS contributions with statistically significant correlations shows that the GS variability is statistically linked with ~25% of the total variability.

The amplitude of EOF Mode-1 in Figure 10 has only a negative sign over the MAB, indicating coherent oscillations of the entire region, but with larger variations in the middle MAB. Table 1 indicates that this mode is highly correlated with the mean current of the entire coast, thus probably related to weather events passing the region, as mentioned before. As seen in Figure 4 and in other cases (not shown), the middle MAB is prone to larger variations when storms pass the region. EOF Mode-2, on the other hand, shows cases when the current speeds in the lower and upper MAB are out of phase with each other, and the time evolution (not shown) indicates wind-induced seasonal variations. To assess the wind influence on Mode-2, the regional wind pattern is shown when the amplitude of Mode-2 was a large positive in January 2021 (Figure 11a) versus a month when the amplitude of Mode-2 was a large negative in September 2021 (Figure 11b). Positive EOF Mode-2 amplitude is associated with strong southeastward wind that is stronger offshore and weaker in the northeast, while negative amplitude is associated with relatively weak eastward wind that is even weaker in the south. This latitudinal change in the wind speed and direction can explain the different impacts on currents in the north and south of the MAB. Mode-2 also has the highest correlation with the GS (Table 1). The direct impact of the GS on the southern portion of the MAB near Cape Hatteras can contribute to the spatial pattern seen in Mode-2 (upper-right panel of Figure 10), with the opposite phase in the upper and lower MAB.

EOF Mode-3 (bottom-left panel of Figure 10) is especially interesting as it shows an opposite amplitude between the shelf-break and the rest of the coast. The location of the shelf-break front

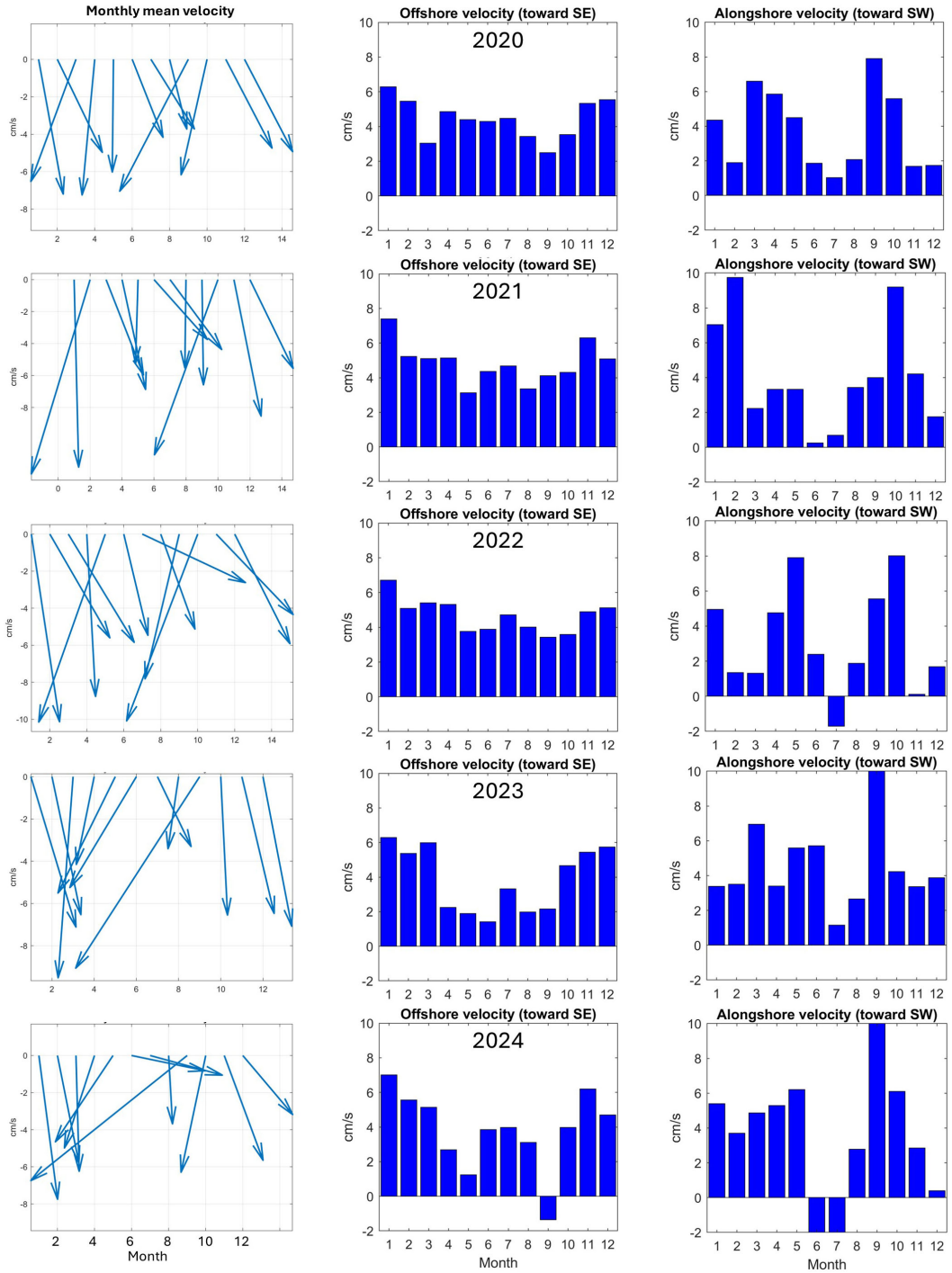

FIGURE 6
Monthly and area mean current velocity of the coastal region for each year (top to bottom). Left panels: mean current vector. Middle panels: offshore velocity component (positive value is a current flowing toward the southeast). Right panels: alongshore velocity component (positive value is a current toward the southwest).

is close to the GS, near the slope sea gyre (Figure 1). To assess the impact of the GS on the shelf-break front, SST images were obtained during two periods: 25 January 25 2021, when Mode-3 in Figure 10 was in a large positive phase (Figure 12a), and 30 September 2023, when Mode-3 was in a large negative phase (Figure 12b). In January 2021, the GS flew straight northeastward and was far from the coast, so the shelf-break front was clearly seen, while in September 2023, the GS had a big meander that reached close to the shelf-break front, which was not clearly visible. This pattern suggests that GS meanders and eddies can impact the shelf-break front as seen in Mode-3. Putting this finding in context, past studies show large variability in the shelf-break front of the MAB that is mostly driven

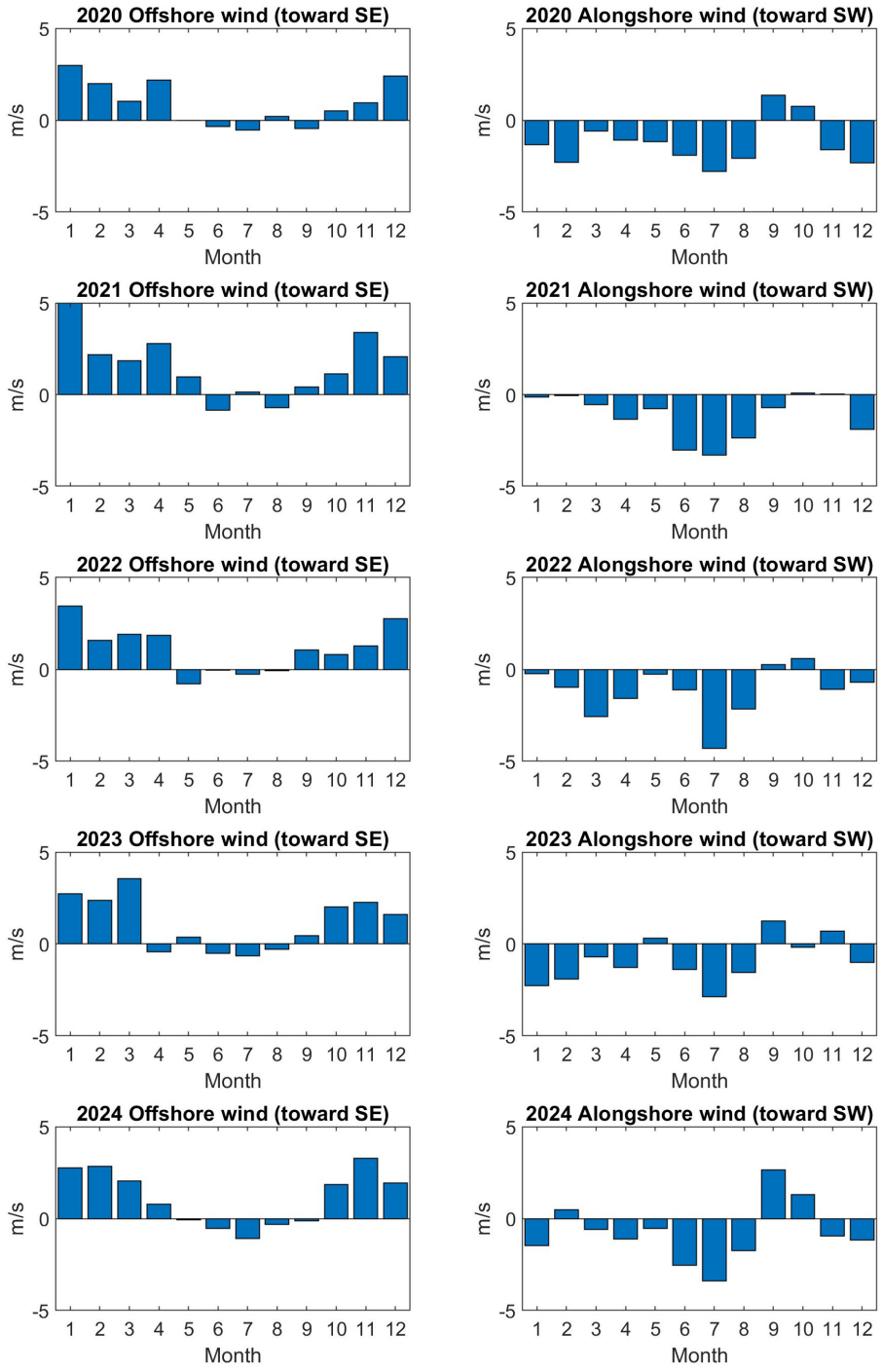

FIGURE 7
Monthly and area mean wind velocity over the study area for each year (top to bottom). Left panels: offshore wind velocity component (positive value is a wind blowing toward the southeast). Right panels: alongshore wind velocity component (positive value is a wind blowing toward the southwest).

by seasonal variations in density gradients (Linder and Gawarkiewicz, 1998). However, some studies also showed cases of an unusual shift in the GS path that brought a GS meander within 12 km from the shelf-break front, such as in December 2011 (Gawarkiewicz et al., 2012), and this unusual case may resemble the GS path in September 2023 (Figure 12b). EOF Mode-4 in Figure 10 shows a pattern where the central MAB near the mouth of Delaware Bay is out of phase with the northern and southern offshore MAB regions—this is the area where the currents near the coast are toward the southeast (Figure 1b) and affected by the outflow from bays (Muscarella et al., 2011; Ezer and Updyke, 2024, 2025). The time evolution of Mode-4 (not shown) indicates an extreme peak in early January 2024 when a strong winter storm hit the northeastern U.S. coast, causing significant snow and flooding.

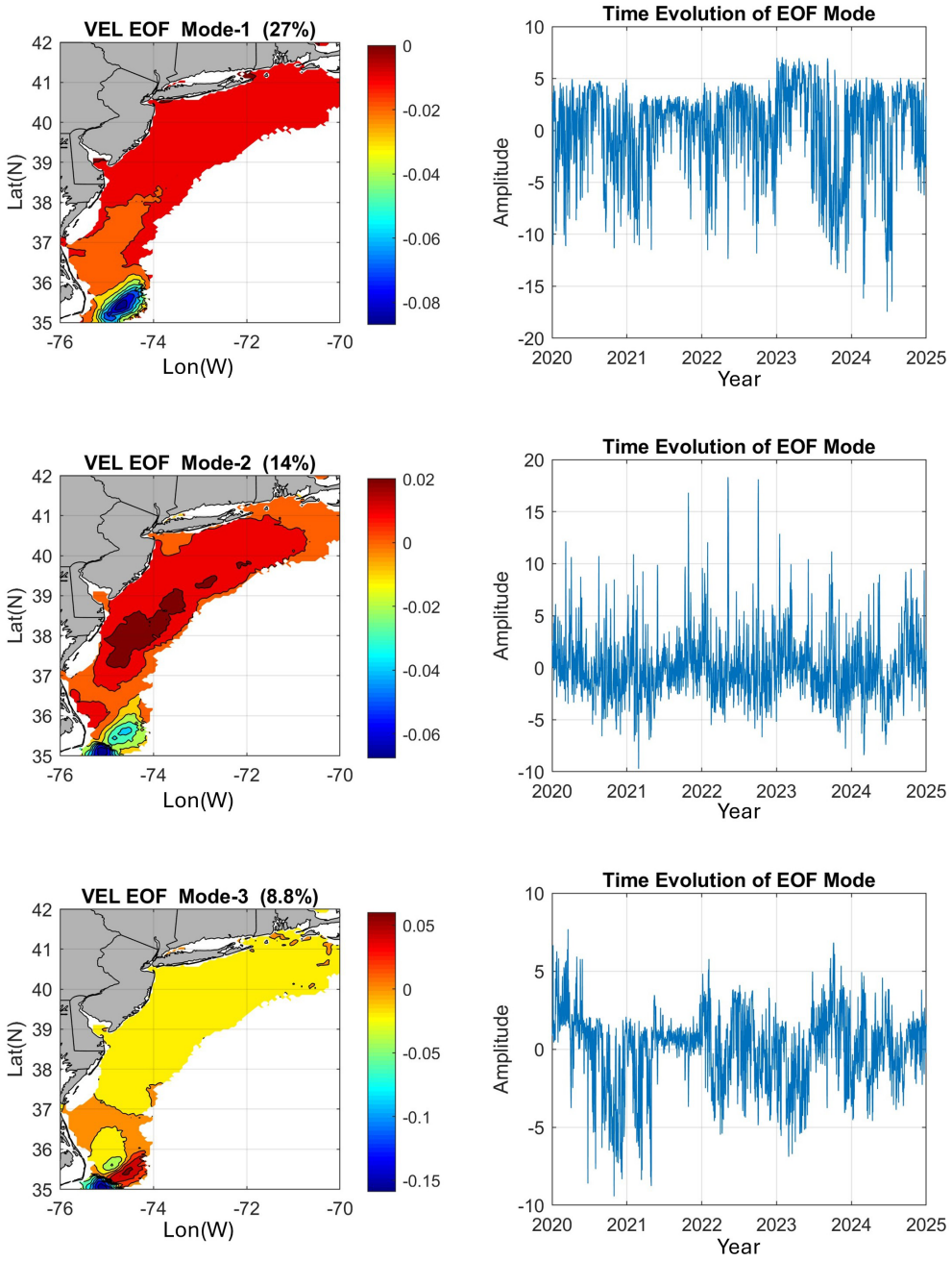

FIGURE 8
The first three modes of empirical orthogonal function (EOF) analysis of the surface current speed—left panels are the spatial pattern (normalized non-dimensional values) and right panels are the time evolution of each mode. The percentage of total variability is indicated for each mode.

For example, USGS observations of the streamflow into the Chesapeake Bay (https://www.usgs.gov/media/images/estimated-monthly-mean-streamflow-entering-chesapeake-bay) show much larger transport in early 2024 than in previous years. However, river discharge has only a minor impact on the overall flow of the MAB away from the coast (Roarty et al., 2020).

To further look at the potential links between the GS and the HFR surface currents, monthly geostrophic velocity obtained from satellite altimeter data was analyzed over 3 years (2020–2022), focusing on the extension of the GS downstream of Cape Hatteras. From the maximum geostrophic velocity at each longitude, the mean latitude of the GS and the mean velocity were calculated between 70°W and 75°W for each month. The seasonal pattern of the GS position and velocity is shown in Figure 13. Due to the large variability of the GS over this region, the seasonal pattern is different for each of the 3 years, so one cannot link the seasonal pattern of the coastal currents to potential seasonal variations in the GS, at least not based on these 3-year data. However, as seen in Figure 12, an occasional shift onshore of the GS may impact the coastal currents. To demonstrate this potential link, 2 months are chosen based on Figure 13: April 2021, when the GS current was strong and its position was farther south, and

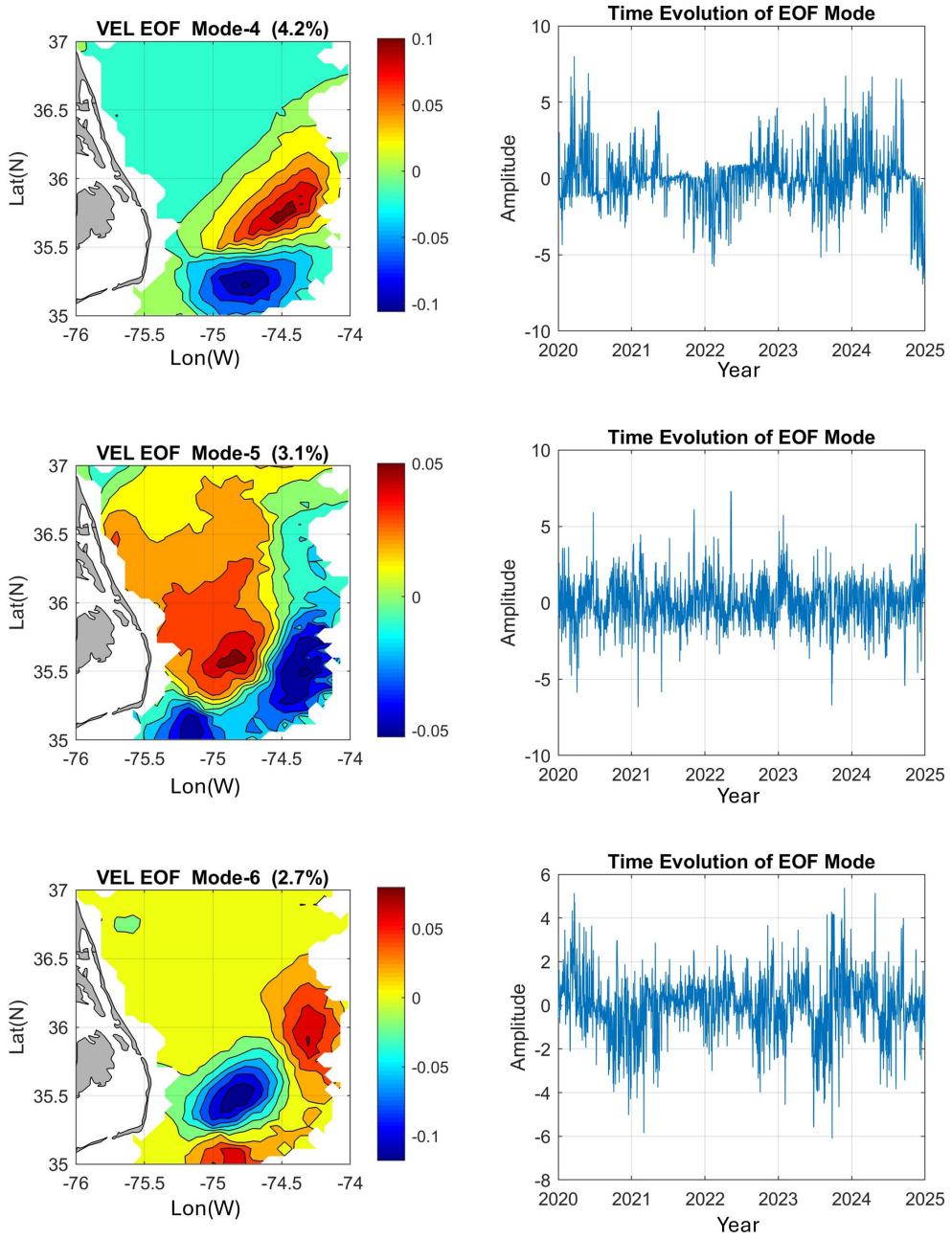

FIGURE 9
As in Figure 8, but for EOF Mode-4 to Mode-6, zooming on the southwest corner of the domain.

November 2021, when the GS current was weak and its position was farther north. The HFR surface currents and the altimeter geostrophic currents are thus compared for the two periods in Figure 14. It is interesting to note that when the GS was strong, the HFR captured a larger portion of the GS. Near the coast, the altimetry-derived geostrophic velocity is noisy and very different from the southeastward observed surface flow, a problem demonstrated by other studies (e.g., Roesler et al., 2013; Caballero et al., 2020). This is not surprising given the fact that coarse-resolution gridded altimetry data are less reliable close to the coast. The currents near the coast are driven by river flow out of bays and local wind, so they are far from being geostrophic or easily detected by sea-level gradients. However, the impact of the GS is seen offshore. When the GS was farther south in April 2021, there was a strong westward geostrophic flow north of the GS, while in November 2021, there seems to be an anticyclonic eddy centered approximately 71°W and 39.5°N; these features are far offshore from the HFR observations. Some impact of the GS on the HFR currents is seen in the southern part of the MAB—when the GS was weaker, there were stronger southwestward currents along the slope and southeastward flow from the mouth of the Chesapeake Bay toward Cape Hatteras. This comparison suggests that combining surface currents from different sources may provide a better data set than each source alone (Caballero et al., 2020).

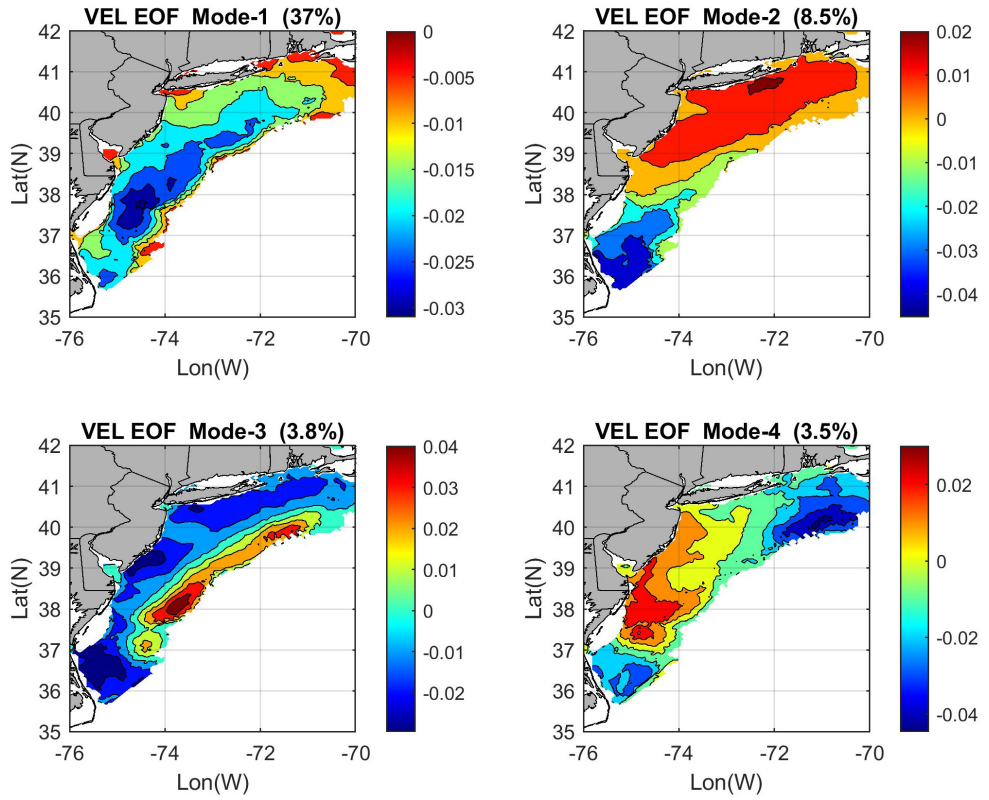

FIGURE 10
EOF modes as in Figures 8 and 9, but only for the coastal area when calculations exclude the Gulf Stream region.

4 Summary and discussion

This research followed the footsteps of past studies that used HFR observations of surface currents along the U.S. East Coast (Kohut et al., 2006; Atkinson et al., 2009; Dzwonkowski et al., 2009; Gong et al., 2010; Muscarella et al., 2011; Gopalakrishnan and Blumberg, 2012; Roarty et al., 2020; Ezer et al., 2022; Han et al., 2022; Seim et al., 2022; Ezer and Updyke, 2024, 2025). However, most of these studies only used local HFR data over a small area near the coast or near the mouth of bays, while here, like in Roarty et al. (2020), the surface currents from multiple radars are used to describe the dynamics and forcing of the entire MAB from Cape Hatteras to Cape Cod. Wind- and river-driven currents of the MAB are well documented in all the above studies, and the results presented here are consistent with past studies. However, there are very few studies that looked at the influence of the GS on coastal currents in the entire MAB, so the goal here was to investigate the potential role that the GS may play in the surface currents of the MAB relative to the (better-known) role of the wind. This is a challenging task since the HFR only captures a small portion of the GS when it flows close to Cape Hatteras. Studies of the GS from HFR data near Cape Hatteras (Haines et al., 2017; Han et al., 2022; Muglia et al., 2022; Seim et al., 2022) demonstrate the role of the GS in water exchange with the shelf; they also found current variability modes associated with wind variability. However, studies focused on the GS near Cape Hatteras alone cannot describe the impact of the GS on the entire MAB. In the deep MAB after the GS separated from the coast at Cape Hatteras, the GS is too far from the coast to be observed by coastal radars—it is also more variable with meanders and eddies than upstream before the separation.

TABLE 1 Correlation between time series of EOF amplitudes and area averaged daily mean velocity over the coastal area (Figure 3b) and over the Gulf Stream area (Figure 3a); *R*(coast) and *R*(gs) are the absolute values of the correlation coefficient with respect to the two records.

Mode	PER	R(coast)	R(gs)
1	37%	**0.94**	**0.1**
2	8.50%	**0.06**	**0.24**
3	3.80%	**0.08**	**0.14**
4	3.50%	**0.08**	**0.12**
5	2.40%	**0.11**	**0.13**
6	2.10%	0.004	**0.12**
7	1.80%	0.04	**0.13**
8	1.50%	0.005	**0.13**
9	1.20%	0.04	0.004
10	1.10%	0.04	**0.06**

Correlations with a significance level over 95% (p-value < 0.05) are in bold. The EOF was calculated when the data over the GS were excluded (Figure 10). The percentage of the total variability represented by each EOF mode is also indicated (PER).

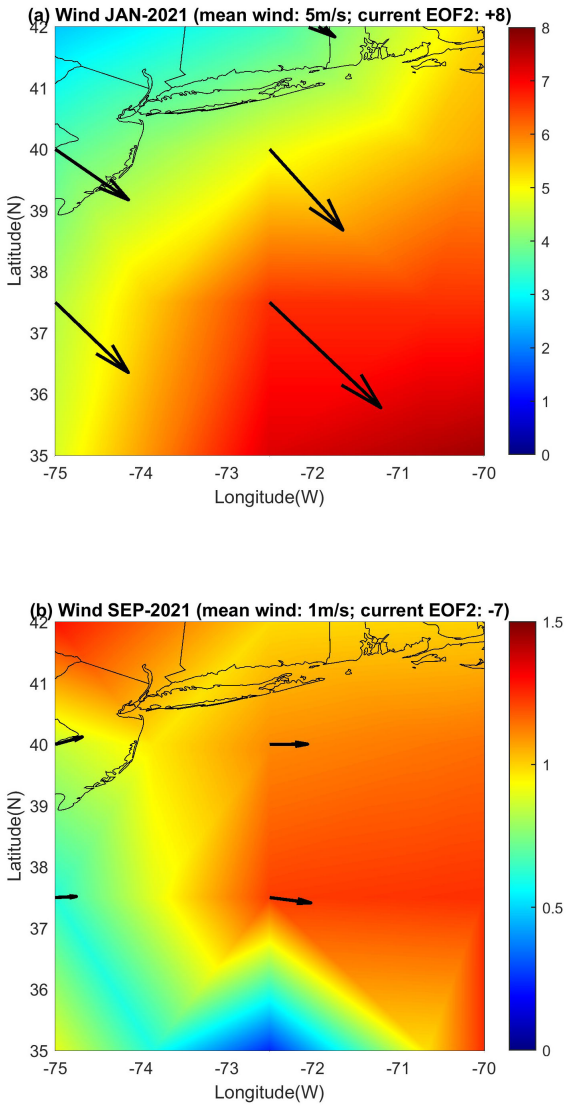

FIGURE 11
The connection between EOF-2 and wind pattern. The monthly mean wind speed (color; in m/s) and direction (vectors) for **(a)** January 2021 and **(b)** September 2021 obtained from the NOAA/NCEP reanalysis. Note the change of wind speed scale between the two panels. These two periods were chosen based on the time evolution of EOF Mode-2 in Figure 10—during the period in **(a)**, EOF-2 had a maximum positive normalized value of +8, while during the period in **(b)**, EOF-2 had a minimum value of −7. Similar connections between EOF-2 and the wind pattern are seen during other times—positive EOF-2 indicates strong offshore wind, while negative EOF-2 indicates very weak wind.

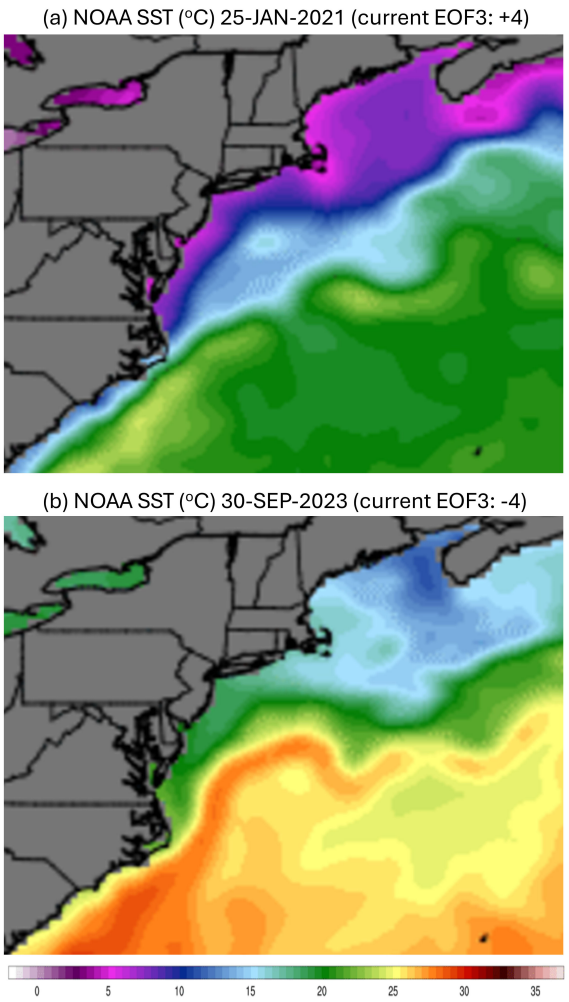

FIGURE 12
The connection between EOF-3, the Gulf Stream (GS), and the shelf-break front. The daily sea surface temperature (SST) for **(a)** 25 January 2021 and **(b)** 30 September 2023. These two periods were chosen based on the time evolution of EOF Mode-3 in Figure 10—during the period in **(a)**, EOF-3 had a maximum positive normalized value of +4, while during the period in **(b)**, EOF-3 had a minimum value of −4. Similar connections between EOF-3 and SST are seen during other times—positive EOF-3 indicates a straight GS path far away from the coast and a strong shelf-break front, while negative EOF-3 indicates GS that meanders toward the coast and erodes the shelf-break front.

Therefore, additional satellite altimeter and SST data were used to characterize the GS path and speed downstream from Cape Hatteras.

Many recent studies focused on the role of the GS and the Atlantic overturning circulation in sea-level variability and coastal sea-level rise (Ezer et al., 2013; Ezer and Atkinson, 2014, 2017; Goddard et al., 2015; Little et al., 2019; Piecuch et al., 2019; Ezer, 2015, 2020, 2022, 2023a; Wu and He, 2025). The mechanism linking the GS with sea-level variability is understood quite well, since variations in the GS position and strength change the location and gradient of the sea-level slope across the GS. However, the mechanism by which GS variability can impact wind-driven velocities near the coast was not clear in past studies. This study, in fact, demonstrates that the impact of the GS on coastal currents is complex and involves several different mechanisms: some directly affect currents in the vicinity of the GS, while others affect the entire MAB or particular locations like the shelf-break.

The main findings about the wind-driven surface currents in the MAB during 2020–2024 are consistent with the results of similar past data until 2016 (Roarty et al., 2020), showing seasonal and interannual variability driven by the seasonal wind pattern of stronger winds in the winter and fall. However, it is further

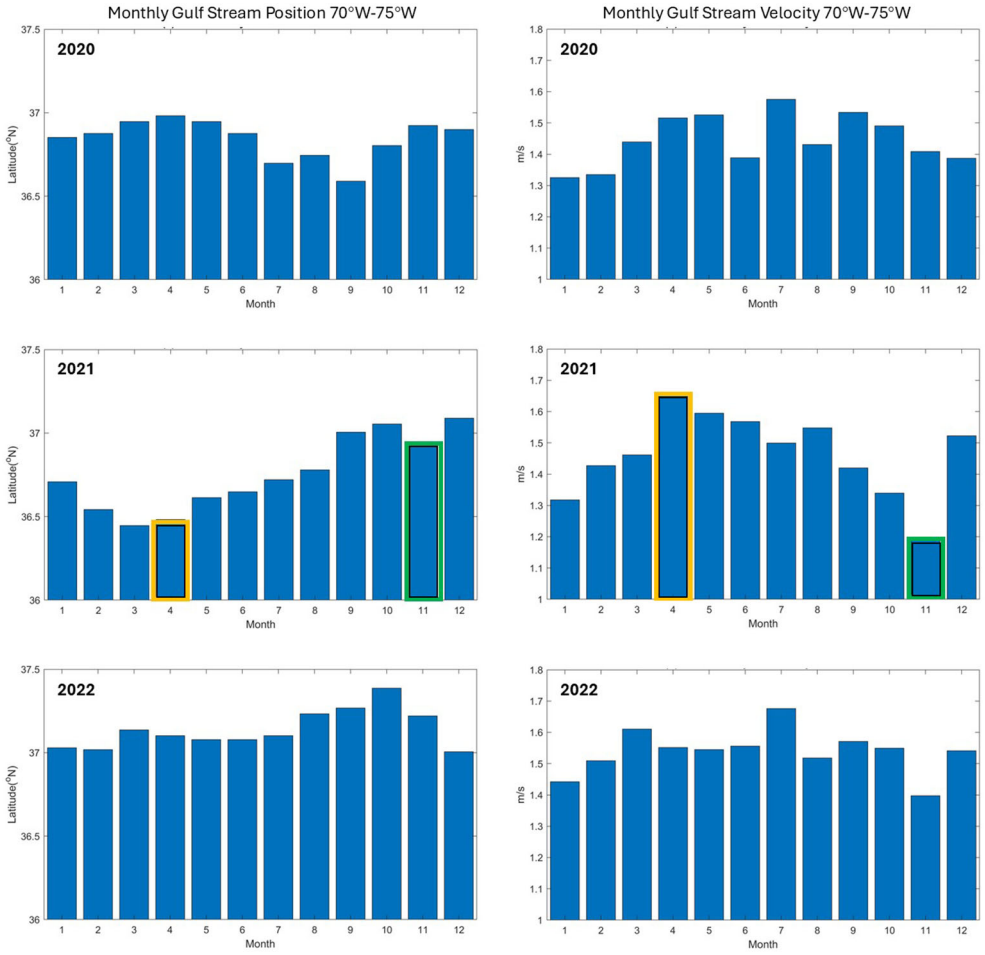

FIGURE 13
Satellite GS variability obtained from geostrophic velocity calculated from satellite altimeter data over 3 years. Left panels: monthly GS mean latitude position. Right panels: monthly GS velocity. The values are averaged over the region 70°W–75°W. Two months are highlighted—April 2021 (orange) when the GS was strong and shifted southward and November 2021 (green) when the GS was weak and shifted northward (see Figure 15).

demonstrated here that HFR data can help study how tropical storms and hurricanes impact the surface currents of the entire MAB region—during storms, mean flow over the MAB can reach over 0.5 m/s, and some locations showed velocity close to 1 m/s (almost GS-like), compared with typical mean current of only 0.1–0.15 m/s. The current direction is generally to the right of the wind as expected from the Ekman theory (Ezer, 2023b)—in fact, a detailed near-coast comparison of wind and currents near the mouth of Chesapeake Bay indicated a 30–50° angle between the wind and surface currents (Ezer and Updyke, 2025). However, farther away from the coast, the currents turn from southeastward to southwestward along the shelf-break front and then merge into the GS closer to Cape Hatteras, as observed by others (Han et al., 2022; Seim et al., 2022). Therefore, away from the coast, the slope sea gyre, the shelf-break front, and the GS path may play a bigger role than just wind. Unlike past studies of the MAB circulation using simple numerical models (Beardsley and Winant, 1979; Beardsley and Haidvogel, 1981) or hydrographic measurements (Linder and Gawarkiewicz, 1998), the HFR provides observations at higher spatial and temporal resolution than was available before and extends from the coast to part of the GS. While the GS dominates the southern portion of the MAB, trying to use the HFR surface currents near the GS to study the link of the GS with coastal currents is very challenging, since the observations capture the small and changing portion of the GS. For example, there are some gaps in the GS data during 2021.

EOF analysis was conducted to study the spatial and temporal pattern of currents in the MAB—one experiment includes both the GS and the coast, and another experiment excludes the GS from the calculations. Patterns that show coherent variability over the entire MAB seem to be driven by a wide range of wind variability: weekly weather events, hurricanes, the seasonal cycle, and interannual variability. However, several EOF modes that capture ~10% of the total variability of the MAB are directly linked with oscillations in the position and strength of the GS near Cape Hatteras. The internal variability in the MAB coastal currents when the GS is excluded

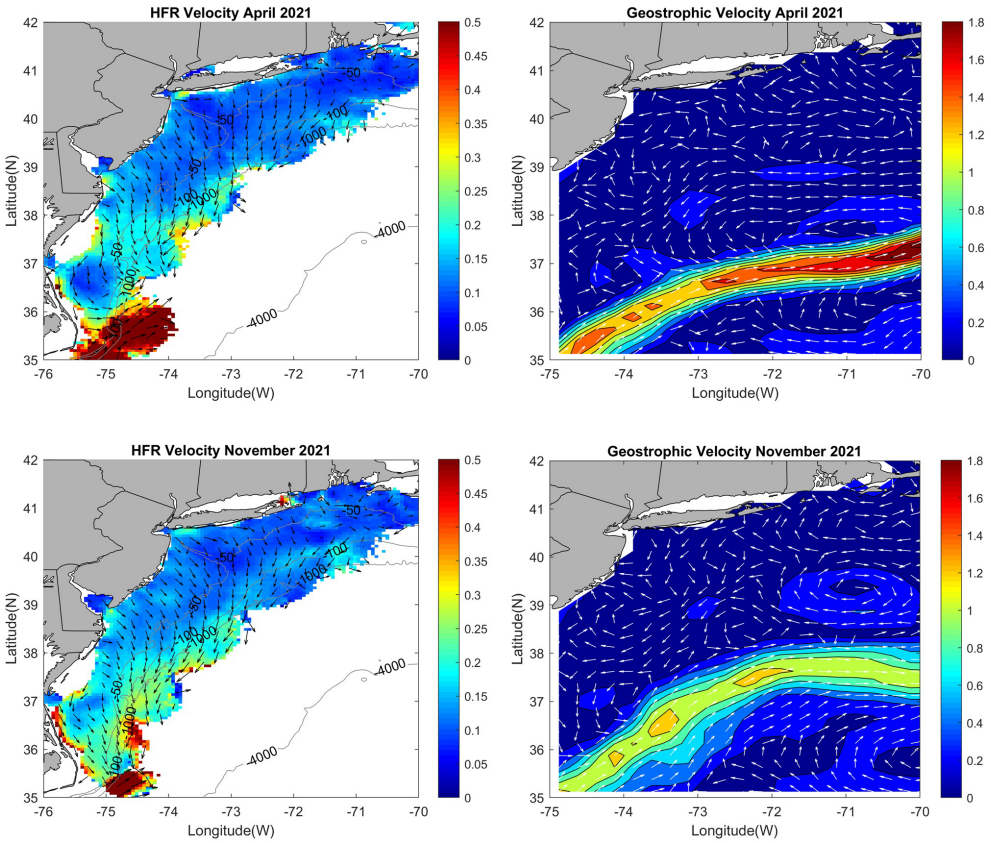

FIGURE 14
A comparison between the observed HFR surface currents (left panels) and the geostrophic surface currents calculated from altimeter data (right panels), for April 2021 (top panels) and November 2021 (bottom panels). These two periods were chosen as examples of different GS patterns, one when the GS is strong and its path is farther south, and one when the GS is weaker, and its path is farther north (see middle panels in Figure 13). The velocity speed (in m/s) is shown by color, and the vectors show direction.

from the calculations shows wind-driven modes with different variations in the upper and lower MAB and a mode associated with variations in the shelf-break front when a GS meander moves closer to the shelf-break. This interaction between the GS and the shelf-break has been seen in observations and can result in an unusual warming of the shelf that affects the ecosystem when a GS meander moves closer to the shelf (Gawarkiewicz et al., 2012). Analysis of the GS extension between 70° and 75°W from altimeter data shows large variations in the GS position and strength, but with no clear seasonal signal; in fact, the seasonal cycle seems different each year. However, qualitatively, large changes in the GS position have a significant impact on the currents in the vicinity of the GS, mostly outside the reach of the HFR observations. Near the coast, however, currents are driven by local wind and river discharge, so geostrophic velocity derived from altimeter data is noisy and does not resemble the observed surface currents. The results thus suggest that the two sources of surface data, direct HRF observations near the coast and geostrophic velocities near the GS, can be combined to provide a better overall flow field than each data alone (Roesler et al., 2013; Caballero et al., 2020) and may also be a source for assimilation into ocean models.

To try to quantify the general contribution of the winds versus the GS on the mean currents of the whole MAB domain, correlations of monthly data were calculated for different years. The link of offshore and alongshore mean currents to the wind components shows correlations that are statistically significant at 99%–99.99% (Figure 15a), which indicates that approximately 50%–80% of the variability (R^2 = 0.5–0.8) is linked to the wind, which is not unexpected. There are, however, interannual variations in the correlations, as discussed before; for example, the alongshore flow had an unusual reversal in the summer and strong fall flow in 2024 (Figure 6) that correlated strongly with a similar wind pattern that year. Much weaker and less consistent correlations were found between the coastal currents and variations in the GS as obtained from altimeter data (Figure 15b). Only the offshore current in some years (but not the alongshore current) had a significant correlation with the GS, indicating that in some years approximately 10%–30% of the variability of the currents is linked to the GS. Since the correlation coefficients in Figure 15b are negative (before squared), it indicates that the offshore component of the coastal currents (toward the southeast) is stronger when the GS moves to the south and is weaker, i.e., the GS is farther away from the coast, so the

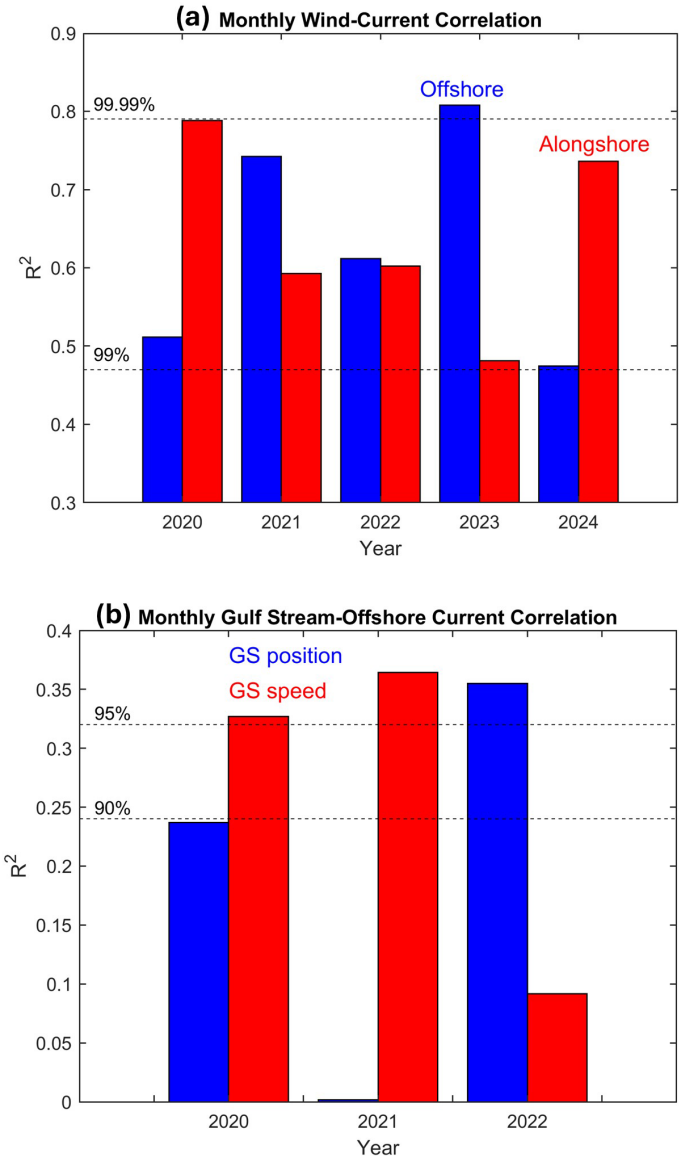

FIGURE 15
Correlation squared (R^2) of monthly surface coastal currents (without the HFR GS) with **(a)** monthly wind and **(b)** the Gulf Stream (from altimeter data). In **(a)**, correlations are separated between offshore components (southeastward; blue) of wind and current and alongshore components (southwestward; red); all correlations (before squared) are positive, i.e., a stronger wind is linked with a stronger current in the same direction. In **(b)**, offshore current component is correlated with GS position (blue) and GS speed (red); alongshore currents are not significantly correlated with the GS, so they are not shown. Correlations (before squared) are negative in **(b)**, i.e., there are stronger offshore currents when the GS is farther south or weaker. Dash lines represent different levels of statistical confidence in the correlation.

currents are likely driven more strongly by the wind with less disruption by the GS. The GS contribution to coastal current variability as obtained from the altimeter data over the MAB (10%–30%; Figure 15b) is consistent with the contribution of the GS obtained from the HFR observations near Cape Hatteras (~25%; Table 1). These two estimates, which were done with different data and different methods, provide confidence in the conclusion that the GS does have a significant impact on the coastal currents.

In summary, the study shows a complex surface current field in the MAB that is driven by variations in both wind and the GS, with variability spanning over a wide range of time and space scales, from daily wind events and storms to seasonal and interannual variations. The study demonstrates the importance of the HFR data to better understand coastal dynamics and interactions between the coast and open ocean dynamics. However, this study, over just a few years, aimed to demonstrate the different processes involved; however, much longer records are needed to quantify the role of the GS in decadal variabilities and climate-related trends in coastal dynamics.

Data availability statement

The original contributions presented in the study are included in the article/supplementary material. Further inquiries can be directed to the corresponding author.

Author contributions

TE: Writing – review & editing, Writing – original draft.

Funding

The author(s) declare that no financial support was received for the research and/or publication of this article.

Acknowledgments

The research is part of ODU's Institute for Coastal Adaptation and Resilience (ICAR). The Center for Coastal Physical Oceanography (CCPO) provided office space and computational support. Special thanks are due to Teresa Updyke, who provided help with the HFR data and comments that helped improve the manuscript. The HFR maintenance work conducted by T. Updyke was funded by NOAA's Mid-Atlantic Regional Association Coastal Ocean Observing System (MARACOOS; Award Number: #NA21NOS0120096). As a graduate of Florida State University, where Bill Dewar spent most of his career, I am honored to contribute this manuscript to the special issue in memory of Bill Dewar—he was a great colleague and a dear friend for many of us.

In memoriam

In memory of William Kurt Dewar: Exploring the dynamics of oceanic boundary currents (e.g., the Gulf Stream) and their impact on weather.

Conflict of interest

The author declares that the research was conducted in the absence of any commercial or financial relationships that could be construed as a potential conflict of interest.

Generative AI statement

The author(s) declare that no Generative AI was used in the creation of this manuscript.

Any alternative text (alt text) provided alongside figures in this article has been generated by Frontiers with the support of artificial intelligence and reasonable efforts have been made to ensure accuracy, including review by the authors wherever possible. If you identify any issues, please contact us.

Publisher's note

References

Atkinson, L. P., Garner, T., Blanco, J., Paternostro, C., and Burke, P. (2009). "HFR surface currents observing system in lower Chesapeake Bay and Virginia coast," in *OCEANS 2009* (IEEE Xplore). Available online at: https://ieeexplore.ieee.org/document/5422254 (Accessed October 26–29, 2009).

Beardsley, R. C., Boicourt, W., and Hansen, D. (1976). "Current variability and mean circulation in Middle Atlantic Bight," in *In trans-AGU*, vol. 57. (AGU Washington DC: American Geophysical Union Publications), 262–262.

Beardsley, R. C., and Haidvogel, D. B. (1981). Model studies of the wind-driven transient circulation in the middle atlantic bight. Part 1: adiabatic boundary conditions. *J. Phys. Oceanogr* 11, 355–375. doi: 10.1175/1520-0485(1981)011<0355:MSOTWD>2.0.CO;2

Beardsley, R. C., and Winant, C. D. (1979). On the mean circulation in the Mid-Atlantic Bight. *J. Phys. Oceanogr* 9, 612–619. doi: 10.1175/1520-0485(1979)009<0612:OTMCIT>2.0.CO;2

Bretherton, C. S., Smith, C., and Wallace, J. M. (1992). An intercomparison of methods for finding coupled patterns in climate data. *J. Clim* 5, 541–560. doi: 10.1175/1520-0442(1992)005<0541:AIOMFF>2.0.CO;2

Caballero, A., Mulet, S., Ayoub, N., Manso-Narvarte, I., Davila, X., Boone, C., et al. (2020). Integration of HF radar observations for an enhanced coastal Mean Dynamic Topography. *Front. Mar. Sci.* 7. doi: 10.3389/fmars.2020.588713

Dangendorf, S., Frederikse, T., Chafik, L., Klinck, J., Ezer, T., and Hamlington, B. (2021). Data-driven reconstruction reveals large-scale ocean circulation control on coastal sea level. *Nat. Clim Change* 11, 514–520. doi: 10.1038/s41558-021-01046-1

Dangendorf, S., Hendricks, N., Sun, Q., Klinck, J., Ezer, T., Frederikse, T., et al. (2023). Acceleration of U.S. Southeast and Gulf coast sea-level rise amplified by internal climate variability. *Nat. Commun.* 14, 1935. doi: 10.1038/s41467-023-37649-9

Domingues, R., Goni, G., Baringer, M., and Volkov, D. (2018). What caused the accelerated sea level changes along the U.S. East Coast during 2010–2015? *Geophy Res. Lett.* 45, 367–13,376. doi: 10.1029/2018GL081183

Dzwonkowski, R., Kohut, J. T., and Yan, X.-H. (2009). Sub-inertial characteristics of the surface flow field over the shelf of the central Mid-Atlantic Bight. *Cont Shelf Res.* 29, 1873–1886. doi: 10.1016/j.csr.2009.07.005

Ezer, T. (2015). Detecting changes in the transport of the Gulf Stream and the Atlantic overturning circulation from coastal sea level data: The extreme decline in 2009–2010 and estimated variations for 1935-2012. *Glob Planet Change* 129, 23–36. doi: 10.1016/j.gloplacha.2015.03.002

Ezer, T. (2020). Analysis of the changing patterns of seasonal flooding along the U.S. East Coast. *Ocean Dyn.* 70, 241–255. doi: 10.1007/s10236-019-01326-7

Ezer, T. (2022). A demonstration of a simple methodology of flood prediction for a coastal city under threat of sea level rise: the case of Norfolk, VA, USA. *Earth's Future* 10. doi: 10.1029/2022EF002786

Ezer, T. (2023a). Sea level acceleration and variability in the Chesapeake Bay: past trends, future projections, and spatial variations within the Bay. *Ocean Dyn* 73, 23–34. doi: 10.1007/s10236-022-01536-6

Ezer, T. (2023b). Evaluation of the applicability of the Ekman theory for wind-driven ocean currents: a comparison with the Mellor-Yamada turbulent model. *Ocean Dyn* 73, 575–591. doi: 10.1007/s10236-023-01570-y

Ezer, T. (2025). The Gulf Stream: its history and links to coastal impacts and climate change. *Annu. Rev. Mar. Sci.* 18. doi: 10.1146/annurev-marine-040224-120037

Ezer, T., and Atkinson, L. P. (2014). Accelerated flooding along the U.S. East Coast: On the impact of sea-level rise, tides, storms, the Gulf Stream, and the North Atlantic Oscillations. *Earth's Future* 2, 362–382. doi: 10.1002/2014EF000252

Ezer, T., and Atkinson, L. P. (2017). On the predictability of high water level along the U.S. East Coast: can the Florida Current measurement be an indicator for flooding caused by remote forcing? *Ocean Dyn* 67, 751–766. doi: 10.1007/s10236-017-1057-0

Ezer, T., Atkinson, L. P., Corlett, W. B., and Blanco, J. L. (2013). Gulf Stream's induced sea level rise and variability along the U.S. mid-Atlantic coast. *J. Geophys Res.* 118, 685–697. doi: 10.1002/jgrc.20091

Ezer, T., and Corlett, W. B. (2012). Is sea level rise accelerating in the Chesapeake Bay? A demonstration of a novel new approach for analyzing sea level data. *Geophys. Res. Lett.* 39, L19605. doi: 10.1029/2012GL053435

Ezer, T., Henderson-Griswold, S., and Updyke, T. (2022). Dynamic observations in the Hampton Roads region: how surface currents at the mouth of Chesapeake Bay may be linked with winds, water level, river discharge and remote forcing from the Gulf Stream. *Oceans 2022 IEEE Xplore*. doi: 10.1109/OCEANS47191.2022.9977092

Ezer, T., and Updyke, T. (2024). On the links between sea level and temperature variations in the Chesapeake Bay and the Atlantic Meridional Overturning Circulation (AMOC). *Ocean Dyn* 74, 307–320. doi: 10.1007/s10236-024-01605-y

Ezer, T., and Updyke, T. (2025). Comparing surface currents near the mouth of three bays along the U.S. *East Coast: Chesapeake Bay Delaware Bay New York Bay Ocean Dyn* 75. doi: 10.1007/s10236-024-01656-1

Gawarkiewicz, G., Todd, R., Plueddemann, A., Andres, M., and Manning, J. P. (2012). Direct interaction between the Gulf Stream and the shelfbreak south of New England. *Sci. Rep.* 2, 553. doi: 10.1038/srep00553

Goddard, P. B., Yin, J., Griffies, S. M., and Zhang, S. (2015). An extreme event of sea-level rise along the Northeast coast of North America in 2009–2010. *Nat. Commun*. doi: 10.1038/ncomms7346

Gong, D., Kohut, J. T., and Glenn, S. M. (2010). Seasonal climatology of wind-driven circulation on the New Jersey Shelf. *J. Geophys Res.* 115, C04006. doi: 10.1029/2009JC005520

Gopalakrishnan, G., and Blumberg, A. F. (2012). Assimilation of HF radar-derived surface currents on tidal-timescales. *J. Oper Oceanogr* 5, 75–87. doi: 10.1080/1755876X.2012.11020133

Haines, S., Seim, H., and Muglia, M. (2017). Implementing quality control of high-frequency radar estimates and application to Gulf Stream surface currents. *J. Atmos Ocean Tech* 34, 1207–1224. doi: 10.1175/JTECH-D-16-0203.1

Han, L., Seim, H., Bane, J., Savidge, D., Andres, M., Gawarkiewicz, G., et al. (2022). Ocean circulation near Cape Hatteras: Observations of mean and variability. *J. Geophys Res. Oceans* 127, e2022JC019274. doi: 10.1029/2022JC019274

Hurrell, J. W. (1995). Decadal trends in the North Atlantic Oscillation: Regional temperatures and precipitation. *Science* 269, 676–679. doi: 10.1126/science.269.5224.676

Kohut, J. T., Glenn, S. M., and Paduan, J. D. (2006). Inner shelf response to tropical storm Floyd. *J. Geophys Res. Oceans* 111. doi: 10.1029/2003JC002173

Le Traon, P. Y., Dibarboure, G., and Dorandeu, J. (2003). SSALTO/DUACS and operational altimetry. In IGARSS 2003. 2003 IEEE International Geoscience and Remote Sensing Symposium. *Proc. (IEEE Cat. No. 03CH37477)* 2, 824–826). doi: 10.1109/IGARSS.2003.1293932

Linder, C. A., and Gawarkiewicz, G. (1998). A climatology of the shelfbreak front in the Middle Atlantic Bight. *J. Geophys Res. Oceans* 103, 18405–18423. doi: 10.1029/98JC01438

Little, C. M., Hu, A., Hughes, C. W., McCarthy, G. D., Piecuch, C. G., Ponte, R. M., et al. (2019). The relationship between U.S. East coast sea level and the atlantic meridional overturning circulation: A review. *J. Geophys Res.* 124, 6435–6458. doi: 10.1029/2019JC015152

Moat, B. I., Smeed, D. A., Rayner, D., Johns, W. E., Smith, R., Volkov, D., et al. (2023). Atlantic meridional overturning circulation observed by the RAPID-MOCHA-WBTS (RAPID-Meridional Overturning Circulation and Heatflux Array-Western Boundary Time Series) array at 26N from 2004 to 2022 (v2022.1), British Oceanographic Data Centre - Natural Environment Research Council, UK. doi: 10.5285/04c79ece-3186-349a-e063-6c86abc0158c

Muglia, M., Seim, H., and Taylor, P. (2022). Gulf Stream position, width, and orientation estimated from HF radar radial velocity maps off Cape Hatteras, North Carolina. *J. Atmos Ocean Tech.* 39, 689–705. doi: 10.1175/JTECH-D-21-0098.1

Muscarella, P. A., Barton, N. P., Lipphardt, B. L. Jr., Veron, D. E., Wong, K. C., and Kirwan, (2011). Surface currents and winds at the Delaware Bay mouth. *Cont Shelf Res.* 31, 1282–1293. doi: 10.1016/j.csr.2011.05.003

Oey, L. Y., Ezer, T., and Sturges, W. (2004). Modeled and observed Empirical Orthogonal Functions of currents in the Yucatan Channel. *J. Geophys Res.* 109, C08011. doi: 10.1029/2004JC002345

Park, K., Di Lorenzo, E., Zhang, Y. J., Wang, H., Ezer, T., and Ye, F. (2024). Delayed coastal inundation caused by ocean dynamics post-hurricane Matthew. *NPJ Clim Atmos Sci.* 7, 5. doi: 10.1038/s41612-023-00549-2

Park, K., Federico, I., Di Lorenzo, E., Ezer, T., Cobb, K. M., Pinardi, N., et al. (2022). The contribution of hurricane remote ocean forcing to storm surge along the Southeastern U.S. coast. *Coast. Eng.* 104098. doi: 10.1016/j.coastaleng.2022.104098

Piecuch, C. G., Dangendorf, S., Gawarkiewicz, G. G., Little, C. M., Ponte, R. M., and Yang, J. (2019). How is New England coastal sea level related to the Atlantic meridional overturning circulation at 26°N? *Geophys Res. Lett.* 46. doi: 10.1029/2019GL083073

Rice, K. C., Moyer, D. L., and Mills, A. L. (2017). Riverine discharges to Chesapeake Bay: Analysis of long-term, (1927-2014) records and implications for future flows in the Chesapeake Bay basin. *J. Env. Mng* 204, 246–254. doi: 10.1016/j.jenvman.2017.08.057

Roarty, H., Glenn, S., Brodie, J., Nazzaro, L., Smith, M., Handel, E., et al. (2020). Annual and seasonal surface circulation over the Mid-Atlantic Bight Continental Shelf derived from a decade of High Frequency Radar observations. *J. Geophys Res. Oceans* 125, e2020JC016368. doi: 10.1029/2020JC016368

Roesler, C. J., Emery, W. J., and Kim, S. Y. (2013). Evaluating the use of high-frequency radar coastal currents to correct satellite altimetry. *J. Geophys Res: Oceans* 118, 3240–3259. doi: 10.1002/jgrc.20220

Seim, H. E., Savidge, D., Andres, M., Bane, J., Edwards, C., Gawarkiewicz, G., et al. (2022). Overview of the processes driving exchange at Cape Hatteras program. *Oceanography* 35. doi: 10.5670/oceanog.2022.205

Smeed, D. A., McCarthy, G. D., Cunningham, S. A., Frajka-Williams, E., Rayner, D., Johns, W. E., et al. (2014). Observed decline of the Atlantic meridional overturning circulation 2004-2012. *Ocean Sci.* 10, 29–38. doi: 10.5194/os-10-29-2014

Sweet, W., and Park, J. (2014). From the extreme to the mean: Acceleration and tipping points of coastal inundation from sea level rise. *Earth's Future* 2, 579–600. doi: 10.1002/2014EF000272

Volkov, D. L., Lee, S.-K., Domingues, R., Zhang, H., and Goes, M. (2019). Interannual sea level variability along the southeastern seaboard of the United States in relation to the gyre-scale heat divergence in the North Atlantic. *Geophys Res. Lett.* doi: 10.1029/2019GL083596

Volkov, D., Zhang, K., Johns, W., Willis, J., Hobbs, W., Goes, M., et al. (2023). Atlantic meridional overturning circulation increases flood risk along the United States southeast coast. *Nat. Comm* 14, 5095. doi: 10.1038/s41467-023-40848-z

Wu, T., and He, R. (2025). Gulf stream near cape hatteras modulates sea level variability along the southeastern coast of north america. *Geophys Res. Lett.* 52, e2024GL112776. doi: 10.1029/2024GL112776